THE JOURNAL OF PHYSICAL CHEMISTRY B

Article

Cite This: J. Phys. Chem. B 2020, 124, 110−120

pubs.acs.org/JPCB

DNA Hairpin Hybridization under Extreme Pressures: A Single-Molecule FRET Study

Hsuan-Lei Sung[†,‡,§] and David J. Nesbitt*[,†,‡,§]

[†]JILA, National Institute of Standards and Technology and University of Colorado, Boulder, Colorado 80309, United States

[‡]Department of Physics and [§]Department of Chemistry and Biochemistry, University of Colorado, Boulder, Colorado 80309, United States

ABSTRACT: Organisms have evolved to live in a variety of complex environments, which clearly has required cellular biology to accommodate to extreme conditions of hydraulic pressure and elevated temperature. In this work, we exploit single-molecule Forster resonance energy transfer (FRET) spectroscopy to probe structural changes in DNA hairpins as a function of pressure and temperature, which allows us to extract detailed thermodynamic information on changes in free energy (ΔG°), free volume (ΔV°), enthalpy (ΔH°), and entropy (ΔS°) associated with DNA loop formation and sequence-dependent stem hybridization. Specifically, time-correlated single-photon counting experiments on freely diffusing 40A DNA hairpin FRET constructs are performed in a 50 μm × 50 μm square quartz capillary cell pressurized from ambient pressure up to 3 kbar. By pressure-dependent van't Hoff analysis of the equilibrium constants, ΔV° for hybridization of the DNA hairpin can be determined as a function of stem length (n_{stem} = 7−10) with single base-pair resolution, which further motivates a simple linear deconstruction into additive stem ($\Delta V^\circ_{stem} = \Delta V^\circ_{bp} \times n_{stem}$) and loop ($\Delta V^\circ_{loop}$) contributions. We find that increasing pressure destabilizes the DNA hairpin stem region [ΔV°_{bp} = +1.98(16) cm^3/(mol bp)], with additional positive free volume changes [ΔV°_{loop} = +7.0(14) cm^3/mol] we ascribe to bending and base stacking disruption of the 40-dA loop. From a van't Hoff temperature-dependent analysis of the DNA 40A hairpin equilibria, the data support a similar additive loop/stem deconstruction of enthalpic ($\Delta H^\circ = \Delta H^\circ_{loop} + \Delta H^\circ_{stem}$) and entropic ($\Delta S^\circ = \Delta S^\circ_{loop} + \Delta S^\circ_{stem}$) contributions, which permits insightful comparison with predictions from nearest-neighbor thermodynamic models for DNA duplex formation. In particular, the stem thermodynamics is consistent with exothermically favored ($\Delta H^\circ_{stem} < 0$) and entropically penalized ($\Delta S^\circ_{stem} < 0$) hydrogen bonding but with additional enthalpic ($\Delta H^\circ_{loop} > 0$) and entropic ($\Delta S^\circ_{loop} > 0$) contributions due to loop bending effects consistent with distortion of dA base stacking in the 40-dA linker.

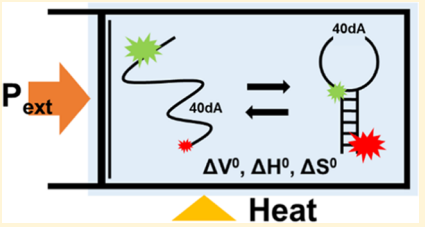

I. INTRODUCTION

Temperature and pressure are two intensive thermodynamic variables that play crucial roles in the folding of biomolecules into biologically competent structures.[1,2] Interestingly, while the thermal dependence of biomolecular conformational change has been thoroughly investigated, the effects of extreme hydraulic pressure have received much less attention. One justification for such disparate attentions is that pressure is a relatively constant variable in conventional biology, while temperature fluctuations are quite common and appreciated to be much more important.[3] However, improved sampling tools in the last 2 decades[4,5] have made extreme biological environments increasingly available for study. As one particularly relevant example, robotic deep-sea exploration vehicles have revealed a plethora of thermophilic organisms thriving in hydrothermal vents where extreme pressures and elevated temperatures result from the rapid increase of hydraulic pressure with ocean depth (≈1 bar every 10 m) and proximity to geothermal heat sources in the ocean bed. In fact, much of the ocean bottom is 3500 m below sea level (i.e., P = 350 bar), with the deepest point in the Marianas Trench at 11 km (i.e., P = 1.1 kbar). From such a perspective, high-pressure biological environments are in fact ubiquitous, with the dynamic range of pressures spanning more than 3 orders of magnitude. This provides incentive for single-molecule biophysical folding studies under extreme (P/T) conditions, with which to explore how biology successfully adapts to (and potentially even harnesses) such extreme variations in pressure and temperature[2,3] to influence conformational folding/unfolding and/or hybridization/dehybridization dynamics.

Pressure and temperature are particularly powerful intensive variables for such thermodynamic exploration. According to the Gibbs free energy differential expression

$$d(\Delta G^\circ) = -\Delta S^\circ(dT) + \Delta V^\circ(dP) \quad (1)$$

the temperature dependence of an equilibrium process is determined by entropy change (ΔS°), while the pressure-dependent response is controlled by the free volume difference (ΔV°) between folded and unfolded conformations.[3,4] In the past decade, spectroscopic methods have been coupled with high-pressure techniques to study local/global changes of biomolecular structures.[1,3] For example, proton-exchange rates

Received: October 28, 2019
Revised: December 7, 2019
Published: December 14, 2019

DOI: 10.1021/acs.jpcb.9b10131
J. Phys. Chem. B 2020, 124, 110−120

in solution-phase NMR spectroscopy have been used to probe pressure-dependent structure formation in proteins,[6,7] while small-angle X-ray scattering experiments have allowed extraction of radii of gyration as a proxy for global compactness as a function of applied pressure.[8−10] Single-molecule Forster resonance energy transfer (FRET) spectroscopy (smFRET, Figure 1) could be particularly useful in detecting conformational change of biomolecules, given the extremely rapid decrease in FRET energy transfer efficiency [$E_{FRET} \sim 1/(1 + (r/r_0)^6)$] with distance between dye-labeled positions, which may therefore be sensitive to conformational compactness,[1,11] as well as overall folding of the biomolecule. Indeed, as external pressure can significantly skew the folding free energy landscape,[12,13] biomolecules can adopt different folding conformations under extreme vs ambient conditions,[11,14] which one could hope to identify by the E_{FRET} value in high-pressure smFRET studies.[11]

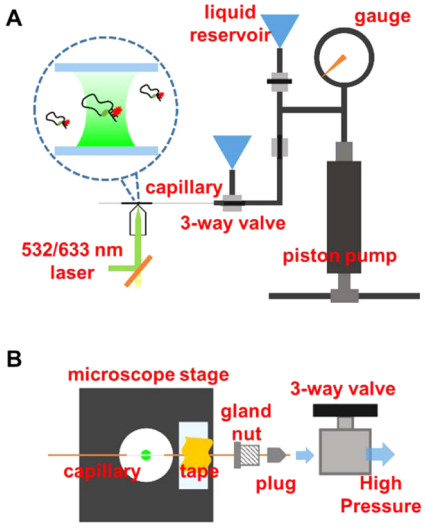

Figure 1. High-pressure smFRET experiment setup: (A) high-pressure-generating system coupled to the confocal microscope for the smFRET freely diffusing study; (B) top view of the square capillary alignment to the microscope objective and the high-pressure mechanical sealing strategy.

The present studies focus on pressure-dependent hybridization/dehybridization of single-molecule DNA hairpins, as a simple first introduction to high-pressure smFRET. DNA hairpins play an important role in biological systems[15] and have been widely used as model constructs for duplex formation, as well as probing the nucleic acid response to cosolutes such as amino acids,[16] osmolytes,[11,14,17] and crowding agents.[18−21] The 40A DNA hairpin construct utilized in the present studies (Figure 2) is ideally suitable for smFRET investigation because (i) folding is known to proceed by well-behaved, unimolecular two-state kinetics[16,18] and yet (ii) the poly(dA) linker acts as a sufficiently long spacer to provide high E_{FRET} contrast between the folded and unfolded conformations. Free volume changes in smFRET DNA hairpin studies have been explored recently, suggesting that the fully hybridized DNA conformation is destabilized (i.e., denatured) with increasing pressure.[11,14,18] While these previous studies have focused on the free volume change ($\Delta V°$) in response to different crowding agents and cosolutes, the effects of sequence, specifically, the dependence of free volume on stem sequence length (n_{step}) and chemical identity (A, T, G, C), have remained largely unexplored. Furthermore, the process of DNA hairpin folding not only requires secondary structure formation in the stem region but also forces the single-stranded DNA loop domain into a more compact ringlike conformation. Since both stem and loop regions represent ubiquitous structural elements in nucleic acid folding,[22,23] the successful deconstruction and simple theoretical modeling of their free volume contributions could provide intriguing, new physical insight into the thermodynamics of the nucleic acid structure.

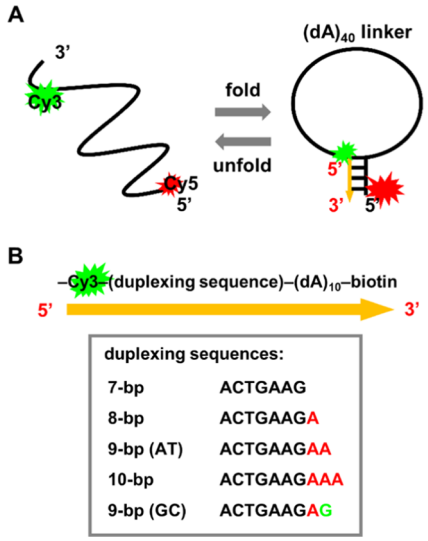

Figure 2. Details of the DNA hairpin smFRET constructs: (A) schematic representation of DNA hairpin folding; (B) structural details of the complementary strand, with systematic variations in the duplexing sequence beyond 7 bp denoted in red (A) and green (G). The location of the Cy3 fluorophore label with respect to the duplexing sequence at the 3′ end is highlighted in green, while the Cy5 fluorophore is covalently attached to the 5′ end.

In this work, we report on the development of new high-pressure smFRET capabilities in our labs with access up to 5 kbar external pressure. We then perform "burst diffusion" smFRET experiments over an extreme pressure (1−3000 bar) and a modest temperature ($\Delta T \approx 10$ K) range, which permit one to extract thermodynamic properties for a series of fluorescently labeled 40A DNA hairpin constructs. For pressure-dependence studies, a manual pressure generator is coupled to a square (50 μm × 50 μm) quartz capillary sample cell (Figure 1), which can sustain from 1 bar up to 5000 bar in pressure without shattering. Such large dynamic ranges in pressure enable measurement of free volume changes (i) at the single molecule level and (ii) with approximately single base-pair resolution. Analysis of the nucleotide-sequence-dependent equilibrium constants for hybridization as well as comparison to nearest-neighbor (NN) predictions[24,25] allows us to extract free volume ($\Delta V°$), enthalpy ($\Delta H°$), and entropy ($\Delta S°$) changes in stem formation, which both isolate and highlight additional contributions to loop formation for each thermodynamic quantity.

The organization of this paper is as follows. In Section II, we present a detailed discussion of the smFRET apparatus, with capabilities for both extreme pressure (1−5000 bar) and modest temperature (20−40 °C) control, with pressure/temperature and sequence-dependent results on 40A DNA hairpin constructs reported in Section III. In Section IV.I, we

DOI: 10.1021/acs.jpcb.9b10131
J. Phys. Chem. B 2020, 124, 110−120

analyze and interpret the stem length and sequence dependence of the high-pressure results and present a simple model for interpreting these data, which permits systematic deconstruction of stem (ΔV_{stem}) and loop (ΔV_{loop}) free volume contributions. In Sections IV.II and IV.III, we explore temperature dependence of 40A hairpin formation, specifically deconstruction of ΔG° into enthalpic and entropic contributions by van't Hoff analysis. The resulting thermodynamic contributions prove consistent with a simple physical picture of (i) exothermic bonding ($\Delta H^\circ < 0$) yet (ii) base stacking in the duplex stem to achieve a more ordered ($\Delta S^\circ < 0$) secondary structure.[26] The results are then compared to nearest-neighbor (NN) model predictions (ΔH_{stem}^{NN}, ΔS_{stem}^{NN}) for DNA stem formation,[24,25] which intriguingly suggest 40-dA loop formation to be endothermic ($\Delta i_{loop} > 0$) and yet favored by entropic gain ($\Delta S_{loop} > 0$). Finally, main conclusions and directions for further experimental improvements are briefly summarized in Section V.

II. EXPERIMENTAL SECTION

II.I. High-Pressure Microscopy Cell and Pressure Control. The current high-pressure smFRET experiments (Figure 1) have been performed by modification of a time-correlated single-photon counting confocal microscope to incorporate a high-pressure glass capillary cell.[27] As one crucial design change, we use square instead of round capillary tubing made from fused silica, with 360 and 50 μm outer and inner diameters, respectively (Polymicro, Phoenix, AZ). This is used to contain the high-pressure sample for microscope studies, with thickness and relatively flat surfaces to mimic a standard coverslip and thereby optimize collection of fluorescent photons.[14] Although studies have previously warned that such square capillaries might fail at pressures over 2 kbar,[27] we find this not to be the case, working well beyond this limit and indeed up to nearly 5 kbar without signs of fracturing. However, we have learned that sealing the capillary end with an oxy-propane torch can at times result in breakage at high pressure, likely due to unresolved strain in the fused silica due to intense heating (and cooling). In our experience, such problems are mitigated by a simple tempering of the glass capillary ends, as described below.

First of all, one end of the capillary is glued with epoxy adhesive into a modified stainless steel pressure plug (High Pressure Equipment, Erie, PA) with a 450 μm hole drilled through the center (Figure 1B) and the opaque outer polymer coating of the capillary removed by a low-temperature propane flame to create optical access for the fluorescent measurements. Loading of the low-concentration DNA samples is then achieved by immersing one end of the capillary into the sample hairpin solution. Once the capillary is filled by capillary action, the free end opposite the plug is sealed with an oxy-propane torch. Since the mechanical strength of the fused silica can be compromised by heating/cooling, we utilize an extended heating time to create an inner channel tapered into a needlepoint in the interior of the glass, thereby reducing the contact surface area and thus the total force on the sealed end. Prior to coupling to the high-pressure liquid source, the plug-attached open end of the capillary is dipped into low-viscosity silicone oil to create a thin immiscible layer, which prevents contamination of the fluorescence capillary region by the pressure-transmitting fluid and yet still conducting the pressure effectively. The sample is then connected to the high-pressure source system by tightening the high-pressure plug and gland nut, during which the flat surface of the square capillary is visually aligned with the microscope objective eyepiece. Since the capillary rotates slightly with the gland nut while being tightened, a coverslip is attached to the capillary with tape to mark the correct capillary orientation (Figure 1B). After tightening the gland nut, the coverslip is then rotated back to the desired flat surface orientation, gently torqueing the capillary to realign its flat surface with the microscope objective. Although this last step might seem practically equivalent to fixing the capillary orientation before tightening the gland nut, the sudden rotation tends to loosen the tape and misalign the capillary. Indeed, strong adhesives may also work well, though we find the tape method easier and faster to apply.

The source of high pressure is simply a manually operated piston screw pump (High Pressure Equipment), which can generate pressures up to 5 kbar (Figure 1A). As adapted from previous works,[27,28] the pressure generator is connected to the sample cell and a Bourdon pressure gauge via high-pressure 1/4 in. stainless steel tubing (High Pressure Equipment), with the entire system filled with ethanol as the pressure-transmitting fluid. Residual air bubbles in the ethanol decrease the pressuring efficiency, which are removed by repeatedly flushing the system through liquid ethanol reservoirs (Figure 1A). The valves are then closed to isolate the fluid reservoirs, with simple mechanical rotation of the piston, achieving the desired pressure (0−5 kbar), as indicated by the Bourdon pressure gauge.

II.II. Temperature Control. Precise temperature control (±0.1 °C) is achieved by simultaneously heating the capillary sample and the microscope objective and stabilizing the temperature with an electronic feedback loop. Prior to each temperature-controlled experiment, the sample holder is mounted on a stage heater (Instec, Boulder, CO) and stabilized via feedback control for more than 15 min to ensure complete thermal equilibrium. At the same time, the microscope objective is heated by a resistive collar (Bioptechs, Butler, PA) to the same temperature to prevent thermal gradients due to water immersion optics. Details of the resistive feedback heating system can be found elsewhere.[29,30]

II.III. DNA 40A Hairpin Construct and Sample Preparation. All DNA hairpin constructs in this study contain the identical 40-nucleotide poly-deoxyadenosine linker (designated as 40A hairpin), with the number of base pairs within the stem varying from n_{stem} = 7−10. The overall construct design, doubly fluorophore-labeled positions, and stem sequences are described in Figure 2, with each of the DNA oligomers commercially available in high-performance liquid chromatography (HPLC) purified forms (Integrated DNA Technologies, Coralville, IA). In the "folded" state of the hairpin, the stem is fully hybridized by complementary Watson−Crick base pairing, bringing the two fluorescent dyes Cy3 and Cy5 in close proximity to achieve the high E_{FRET} (~0.8) state. Conversely, dissociation of the duplex stem "unfolds" the hairpin, which allows the covalently linked dye-labeled strands to diffuse to much larger (~80 Å) separations, resulting in an E_{FRET} state near zero. The observed range of E_{FRET} values is entirely consistent with predictions based on the Cy3/Cy5 Forster radius (R_0 = 55 Å), construct geometry, and results from previous surface-tethered smFRET experiments.[16] There is a 10-dA-biotin oligo extension on the 3′ end after the duplexing sequence, designed for future attachment of the 40A hairpin constructs to a bovine serum albumin (BSA) surface by biotin−streptavidin interactions. For simplicity in

DOI: 10.1021/acs.jpcb.9b10131
J. Phys. Chem. B 2020, 124, 110−120

these first high-pressure experiments, however, we have simply chosen to allow the constructs to freely diffuse in solution through the laser beam, exploiting "burst fluorescence" methods to stochastically probe the single 40A hairpin oligos present in the confocal volume.

In preparation of the smFRET samples, the stock DNA solution has been diluted in imaging buffer to ~50 pM, such that fluorescent bursts result exclusively from single doubly labeled DNA constructs diffusing through the confocal volume. The imaging buffer contains (i) 50 mM hemipotassium *N*-(2-hydroxyethyl)piperazine-*N*′-ethanesulfonic acid (HEPES) buffer (pH 7.5), (ii) Trolox/protocatechuate 3,4-dioxygenase (PCD)/protocatechuate (PCA) oxygen scavenger cocktail to catalytically remove oxygen[16,30] and thereby increase Cy3/Cy5 dye photostability, with (iii) sufficient NaCl to achieve total monovalent cation concentrations of $[M^+]$ = 100 mM.

II.IV. Single-Molecule FRET Spectroscopy and Data Analysis. Details of the confocal smFRET experimental apparatus can be found in previous works.[30−32] In short, the output from a 532 nm Nd:YAG laser (10 ps pulses at a 20 MHz repetition rate) is beam expanded, collimated, and directed into an inverted confocal microscope with a 1.2 N.A. water immersion objective. The collimated beam overfills the limiting microscope aperture, resulting in a near-diffraction-limited excitation and collection spot size [$1/e^2$ radius ω_0 = 310(30) nm]. In the current smFRET diffusion experiments (Figure 1A), the laser is focused into a solution of doubly dye-labeled 40A DNA at sufficient dilution (~50 pM) to ensure that only a single DNA molecule diffuses through the observation window at a time, thereby generating typically an isolated ≈1 ms burst in the fluorescent signal (Figure 3A,B). The resulting photons are collected through the same objective and sorted by wavelength (green/red) and polarization (horizontal/vertical) before detection on four single-photon avalanche photodiodes (APDs). A 50 μm pinhole spatial filter before the APD detection unit is used to restrict out-of-focus photons along the (z) photon propagation direction to achieve a subfemtoliter detection volume. For each fluorescent burst above the 25 kHz photon/s software adjustable count rate threshold (i.e., 10-fold higher than background noise in an equivalent 1 ms burst window), an E_{FRET} value is obtained from the number of green vs red photon counts detected, after suitable correction for background and crosstalk contributions with in-house software.[31,33] Since the double fluorophore labeling efficiency for the DNA constructs is high but imperfect (>90%), alternating laser excitation (ALEX) methods with interleaving green and red laser pulses are used to ensure that only bursts from doubly labeled DNA constructs are included in the E_{FRET} distributions.[31,34] By way of example, the series of events flagged by arrows in Figure 3B and numbered from 1 to 4 can be unambiguously sorted into fluorescent bursts corresponding to (1) unfolded yet doubly labeled, (2) Cy3-only-labeled, (3) Cy5-only-labeled, and (4) folded doubly labeled DNA constructs, respectively.

Once the E_{FRET} value of each burst event from doubly labeled DNA has been computed, an E_{FRET} histogram is generated (Figure 3C). Note that the E_{FRET} value is calculated as $I_A/(I_A + I_D)$, where $I_{A/D}$ is the total acceptor/donor signal after background fluorescence and detector crosstalk corrections. For the DNA hairpin constructs in this study, the E_{FRET} histograms exhibit two distinct populations with low E_{FRET} (~0) and high E_{FRET} (~0.8), corresponding to the unfolded and folded conformations, respectively.[16] The E_{FRET} distribution is then fit to a sum of two Gaussian functions, with the folding equilibrium constant readily calculated from the ratio of areas under each component.[29,31,33,34] We have observed for each hairpin construct the maximum folded fraction to be around 80%. This actively folding fraction is consistent with our surface-tethered smFRET experiments, for which 80% of the DNA hairpin constructs actively fold/unfold, with the remainder being trapped in the low E_{FRET} configuration. Quantification of the nonfolding subpopulation is thereby achieved by comparing surface-tethered results with freely diffusing studies,[29,33] with such subpopulations subtracted from the equilibrium constant calculation, as detailed in

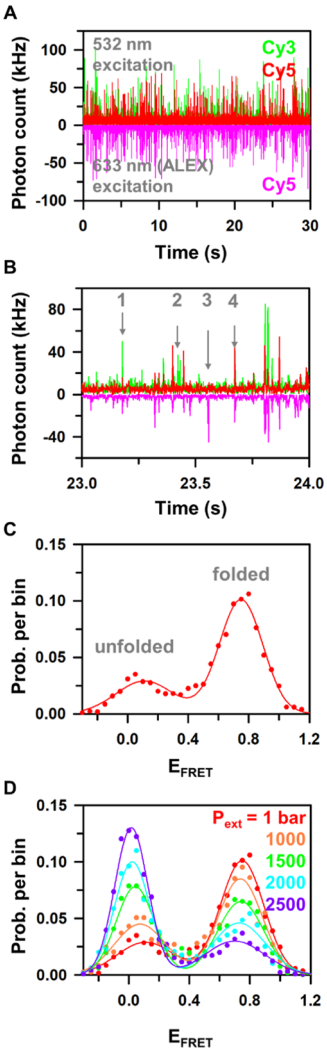

Figure 3. Sample data and analysis from the freely diffusing smFRET studies: (A) sample time-resolved fluorescent signals from 532 nm laser excitation, with upward green and red traces corresponding to Cy3 and Cy5 fluorescence channels, respectively. The pink trace due to the 633 nm alternating laser excitation (ALEX) of the diffusing constructs is plotted downward for direct comparison with the 532 nm excitation signals, confirming the presence (or absence) of the Cy5 fluor. (B) Single events in the fluorescence traces, where arrows point to the fluorescent bursts corresponding to (1) an unfolded doubly labeled hairpin, (2) a Cy3-only, (3) Cy5-only, and (4) folded doubly labeled construct. (C) Sample E_{FRET} histogram of the 9 bp (AT) hairpin folding at ambient pressure, fit to a superposition of two Gaussians. (D) Sample E_{FRET} histogram of the 9 bp hairpin folding at a series of external pressures, revealing a reversible propensity for unfolding with increasing P_{ext} (1−2500 bar).

DOI: 10.1021/acs.jpcb.9b10131
J. Phys. Chem. B 2020, 124, 110−120

previous works.[29,33] The resulting folding equilibrium constant (K_{fold}) is then obtained from this corrected data and used for further thermodynamic analyses.

III. RESULTS AND ANALYSIS

III.I. Pressure Dependence of DNA Hairpin Folding.

The free volume taken up by a biomolecule will vary as a function of conformation, which in turn will control the effect of external pressure on biomolecular folding.[3,4] By differentiating the expression for Gibbs free energy, we can express the pressure dependence of the folding equilibrium constant as[3]

$$\left(\frac{\partial \ln K_{fold}}{\partial P}\right)_T = \frac{-\Delta V^\circ}{RT} \tag{2}$$

where R is the gas constant and ΔV° denotes the change in free volume upon folding: $\Delta V^\circ = V_{fold} - V_{unfold}$. According to eq 2, folding is promoted by increasing pressure when $\Delta V^\circ < 0$, and reduced by pressure when $\Delta V^\circ > 0$. As expected from Le Chatelier's principle, stress due to increasing pressure is partially relieved by shifting the equilibrium toward the direction of smaller volume.[3] Equation 2 can be integrated at constant T to predict the simple function dependence of K_{fold} on external pressure

$$\ln K_{fold}(P) = \frac{-P_{ext}\Delta V^\circ}{RT} + C \text{ or } K_{fold}(P) = \exp\left(\frac{-P_{ext}\Delta V^\circ}{RT} + C\right) \tag{3}$$

where C is the integration constant. Note that C simply reflects a constant offset and is completely independent of the pressure-dependent slopes measured and reported herein.

To explore the pressure dependence of DNA hairpin folding, smFRET experiments have been performed over a wide range of external pressures (P_{ext} = 1−3000 bar) inside fused silica square capillaries coupled to our high-pressure compression apparatus. The sample E_{FRET} histogram reveals two distinct populations with $E_{FRET} \approx 0$ and 0.8 (Figure 3C), corresponding to unfolded and folded states of the DNA hairpin construct, respectively. As the external pressure rises, the folded (unfolded) population decreases (increases), respectively. This implies that increasing pressure favors the unfolded state of the DNA hairpin and thus a positive change in free volume ($\Delta V^\circ > 0$) (Figure 3D). Such pressure-induced unfolding or "denaturation" has been experimentally observed in previous bulk ensemble studies of nucleic acids[35] and proteins.[3,36] However, the physical reason behind why $\Delta V^\circ > 0$ is far from obvious, since one might at first expect nucleic acids and proteins to adopt more compact conformations upon folding. Though still controversial,[36−39] one of the simplest interpretations would be that the folded structure generates more hydrophobic regions, which exclude the solvent shell, generating "solvent voids" and therefore taking up greater volume. An equally plausible explanation is that the increase in solvent-accessible surface area (SASA) of the unfolded state facilitates solvation with a more compact solvent structure, which translates into $\Delta V^\circ > 0$ and thus correctly predicts the pressure-induced denaturation of biomolecules.[36−39]

The pressure dependences of DNA hairpin folding with different stem sequences are plotted in Figure 4A, which display the expected linear dependence (i.e., eq 3) of $\ln[K_{fold}]$ vs P_{ext} and provide clear evidence that the 40A DNA hairpin constructs unfold with increasing pressure. Note the systematic upward shift in these curves with increasing stem sequence length, which is in almost all cases consistent with the exponential increase in K_{fold} predicted with additional free energy release due to incremental base pairing. The only exception to this trend is evident in the nearly overlapping K_{fold} trendlines for the 7 and 8 bp constructs, which occur because the additional stabilization due to the extra base pair (n_{stem} = 7 vs 8) is counteracted by the terminal d(G-C) pair being replaced by the less stable d(A-T) (Figure 2B) in the 7 and 8 bp constructs, respectively.

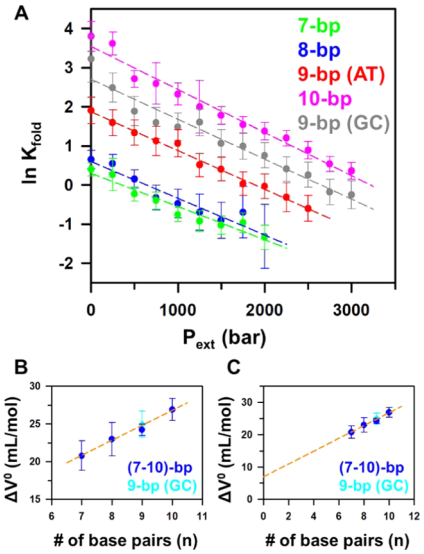

Figure 4. Pressure dependence of folding for a systematic series of DNA hairpins: (A) pressure effects presented in a van't Hoff plot of $\ln[K_{fold}]$ vs P_{ext}, for which the slope yields the free volume change due to DNA stem hybridization ($\Delta V^\circ = V^\circ_{fold} - V^\circ_{unfold}$). (B) Volume changes upon folding (ΔV°) as a function of number of base pairs in the duplex stems, which reveal a remarkable linear dependence on n_{stem}; (C) extrapolation of this linear dependence on stem length to n_{stem} = 0, thereby isolating free volume contributions (ΔV°_{loop}) to DNA hybridization from formation of the 40A loop.

For nearly incompressible fluids, ΔV° remains approximately constant over wide pressure ranges;[36] hence, the data for each stem sequence can be linearly fit to eq 3 to obtain accurate free volume changes upon folding (ΔV°) as a function of hybridization length. Although the slopes appear quite similar for each data set, upon closer inspection, systematic differences are visually apparent. By way of more quantitative comparison, least-squares fitted slopes (ΔV°) of Figure 4A have been plotted against the number of base pairs in Figure 4B,C. Although the slope uncertainties are appreciable, the overall trend in the data is quite clear; ΔV° increases smoothly and quasilinearly with the number of base pairs within the duplex stem. This can be rationalized by a roughly linear growth in solvent-inaccessible "voids" and hydration volume with each additional DNA base pair in the stem sequence. Most importantly, pressure-induced measurements of ΔV° exhibit a sensitivity to stem length that is clearly at the single base-pair level of resolution.

If we interpret this quasilinearity as arising solely from solvent-inaccessible regions in the stem, the data suggest a deconstruction of the free volume change into a simple additive sum of stem and loop contributions with a ΔV°

DOI: 10.1021/acs.jpcb.9b10131
J. Phys. Chem. B 2020, 124, 110−120

resolution close to the single base-pair difference; the average volume change per base pair $\Delta V_{stem} = \Delta V_{bp} \times n_{stem}$ is determined to be $\Delta V_{bp} = 1.98(16)$ cm^3/(mol bp), which is consistent with previous values [$\Delta V_{bp} = 2.1(4)$ cm^3/(mol bp)] obtained from high-pressure UV melting experiments on poly[d(A-T)] DNA.[40−42] Moreover, despite the impressively small fractional uncertainties in $\Delta V°$ obtained from these least-squares fits, the 9 bp hairpin with a weaker terminal d(A-T) base pair is experimentally indistinguishable from the 9 bp hairpin with a stronger terminal d(G-C). Thus, although the incremental free volume changes due to increasing stem length are unambiguously determined in this study, the corresponding effects due to a stronger d(G-C) or weaker d(A-T) terminal base pairing appear to be 5−10-fold smaller and obscure any finer differential effects at our current sensitivities due to single base-pair variance.

III.II. Temperature Dependence of DNA Hairpin Folding. Temperature plays an equally crucial role in both the kinetics and thermodynamics of biochemical reactions, with nucleic acid structures known to be highly sensitive to temperature.[43] In general, nucleic acids fold into more ordered states driven by exothermic interactions such as hydrogen bonding and base stacking. Thus, by Le Chatelier's principle, folding in nucleic acids is generally but not exclusively unfavored by increasing temperature, with notable exceptions in systems where the free energy changes are dominated by solvent vs solute contributions.[32,44,45] The temperature-dependent unfolding of the DNA hairpins is shown in a van't Hoff plot (Figure 5A), where ln[K_{fold}] is plotted as a function of reciprocal temperature ($1/T$). The data are well fit to linear functions, which allow us to deconstruct the full folding free energy ($\Delta G°$) into enthalpic ($\Delta H°$) and entropic ($\Delta S°$) contributions

$$\ln K_{fold} = -\frac{1}{T}\frac{\Delta H°}{R} + \frac{\Delta S°}{R} \quad (4)$$

Note that the fractional temperature vs pressure changes required to see comparable effects in K_{fold} differ by orders of magnitude. This is due to the large change in entropy upon folding of a complex biomolecule, which results in much larger thermodynamic free energy contributions arising from $T\Delta S°$ vs $P\Delta V°$ under ambient physiological conditions. In the linear least-squares fits in Figure 5A, the positive slopes signal folding of the 40A hairpin to be exothermic ($\Delta H° < 0$) and therefore penalized by heating. Conversely, the negative intercepts from these fits indicate a decrease in entropy ($\Delta S° < 0$) during hairpin formation, consistent with the canonical picture (stated above) of folding into a more ordered structure. However, one should always be mindful that the measured thermodynamic response is determined by free energy change for the entire system, which includes structural effects from both the biomolecules and the surrounding solvent.[32,46,47]

Thermodynamic results for $\Delta H°$ and $\Delta S°$ from van't Hoff analysis for the n_{stem} = 7−10 and 9 bp (GC) series of constructs are summarized in Figure 5B,C, along with predictions of the same quantities by nearest-neighbor models.[24,25] Interestingly, these plots explicitly demonstrate that $\Delta H°$ and $\Delta S°$ both decrease in an approximately linearly fashion with the number of base pairs (n_{stem}) (Figure 5B), consistent with a heat release and change in disorder roughly proportional to hybridization length. Also worth emphasizing, the 9 bp hairpin with a terminal d(G-C) base pair exhibits a noticeably larger incremental decrease in both $\Delta H°$ and $\Delta S°$

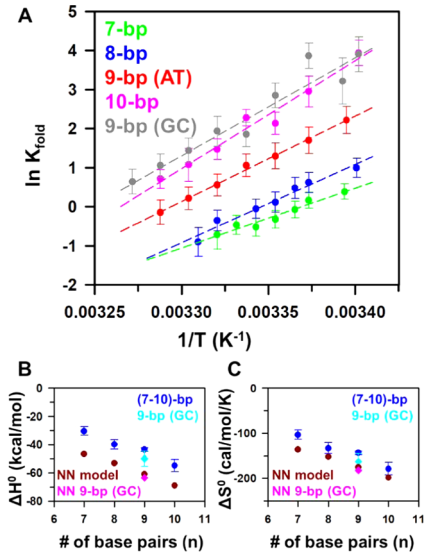

Figure 5. Temperature-dependent folding response: (A) temperature unfolding effects for the series of DNA hairpins presented as a standard van't Hoff plot, with the slope ($m = -\Delta H°$) and intercept yielding the enthalpy and entropy changes upon folding; (B) enthalpy change ($\Delta H°$) as a function of stem length (n_{stem}, dark blue), as well as predictions (dark red) from nearest-neighbor model parameters; (C) entropy change ($\Delta S°$) as a function of duplex stem length (dark blue), in comparison to the nearest-neighbor model prediction for fully bimolecular stem formation (dark red). The two additional points in (B) and (C) (light blue) correspond to data for an alternate 9 bp construct with the 3′ d(A-T) replaced by a stronger d(G-C) base pair. Corresponding enthalpy and entropy predictions from nearest-neighbor model predictions for bimolecular stem formation are also shown (light red), which suggest a small increase in enthalpy and entropy changes under unimolecular stem formation conditions for a hairpin construct.

than for the corresponding 9 bp hairpin sequence with a terminal d(A-T) base pair. This shift arises as a result of a stronger d(G-C) vs d(A-T) base-pairing interaction, consistent with previous observations.[24,25]

IV. DISCUSSION

IV.I. Deconstructing Free Volume Changes into DNA Stem and Loop Formation. With the present experimental combination of (i) high dynamic range of pressures and (ii) quantitative smFRET measurements, we achieve single base-pair resolution for the free volume changes ($\Delta V°$) incurred upon hybridization of a 40A DNA hairpin. Furthermore, when the analysis is repeated for a series of stem junction sequences (Figure 2), the data follow a nearly linear trend with a slope $\Delta V°_{bp} = 1.98(16)$ cm^3/(mol bp) (Figure 4B), which is already consistent with a previously reported (albeit less precise) value of $\Delta V°_{bp} = 2.1(4)$ cm^3/(mol bp) for poly[d(A-T)] DNA hybridization obtained from high-pressure UV melting experiments under comparable monovalent cation concentrations.[40] Although the effect of swapping a single base pair (i.e., 9 bp AT to 9 bp GC) is indistinguishable for the present selection of stem sequences, results from previous high-pressure UV melting studies at a relatively low monovalent cation concentration for poly[d(A-T)], poly[d(G-C)],[48] and poly[d-(I-C)] (dI = 2′-deoxyinosine, a dG-like derivative) yield unit base-pair slopes of $\Delta V°_{bp}$ = 1.42, 4.57,[41] and 4.8(6) cm^3/(mol bp),[48] respectively. Specifically, the predicted free volume differences for single d(A-T) and d(G-C) swaps in poly[d(A-

DOI: 10.1021/acs.jpcb.9b10131
J. Phys. Chem. B 2020, 124, 110−120

T)] and poly[d(G-C)] would be $\Delta\Delta V^{\circ}_{bp}$ = 3.4 cm^3/(mol bp). This is significantly higher (20-fold) than our experimental uncertainty, yet no change is seen for such a d(A-T) → d(G-C) single base-pair swap in our data. In contrast, a UV melting experiment of mixed-base-pair DNA with G-C content similar to our complementary sequences has found ΔV°_{bp} = 1.8(2) cm^3/(mol bp),[42] in much improved agreement with our results. We therefore suspect that ΔV_{bp} may additionally depend upon interaction between neighboring base pairs, resulting in excess values of ΔV°_{bp} for homonucleotide duplexes poly[d(G-C)] and poly[d(I-C)], which appear to be moderated in DNA duplexes with more mixed-base-pair character.

If we extrapolate the linear relation between ΔV° and the number of base pairs, the vertical intercept is clearly positive, well within experimental uncertainty (Figure 4C). This indicates that there must be a free volume change ΔV° (0 bp) > 0 even in the absence of any base pairing of the stem sequence. A simple additive model for this behavior would suggest that the overall change in free volume is given by

$$\Delta V^{\circ} = \Delta V^{\circ}_{stem} + \Delta V^{\circ}_{loop} = \Delta V^{\circ}_{bp} \times n + \Delta V^{\circ}_{loop} \quad (5)$$

where ΔV°_{loop} represents a contribution generated from loop formation of the single-stranded poly(dA) DNA linker. Specifically, the results suggest an increase in the effective DNA volume [ΔV°_{loop} = +7.0(14) cm^3/mol] when the DNA linker forms a loop structure,[49,50] which at first seems counterintuitive. However, it is also well established that single-stranded poly(dA) is appreciably structured due to spontaneous base stacking between adjacent adenine bases, a stacking that would be disrupted upon folding of the hairpin[51−55] due to loop distortion. The data therefore suggest that the closely stacked adenine bases occupy less volume than free bases, and therefore when the base stacking is disrupted, the effective volume occupied by the single-strand DNA increases, thus resulting in a positive volume change contributed from DNA linker looping (ΔV°_{loop} > 0).

Although positive ΔV°_{bp} would seem to imply that a longer double-stranded DNA is more susceptible to pressure denaturation effects, we have found the free energy stabilization per base to be more than an order of magnitude higher than the pressure-induced shifts would predict even at the bottom of the Marianas Trench (~1.1 kbar). Thus, we find that the stability of a DNA duplex increases uniformly with the number of base pairs at any pressure. However, such pressure-dependent perturbations could significantly affect the local stability of a DNA double strand, especially when the DNA needs to partially melt (unzip) to participate in biochemical reactions, such as DNA replication and transcription. Interestingly, deep-sea species can also alter cellular osmolyte compositions to accommodate/offset effects due to a high-pressure environment.[56] Indeed, it has been found that deep-sea fish tend to accumulate a high level of trimethylamine *N*-oxide (TMAO) in their muscles,[56,57] which not only stabilizes DNA secondary structures[58] but also reduces ΔV° and thereby mitigates any pressure-dependent effects.[11,18] Most importantly, high pressure may similarly destabilize RNA structures and thereby greatly affect biochemical function. For example, regulatory elements such as RNA riboswitches can be extremely sensitive to pressure, due to the fact that they dynamically fold into different conformations to control gene expression. The deconstructed volume contributions from stem (ΔV°_{stem}) and loop (ΔV°_{loop}) determined in this work should help in predicting pressure-dependent results from more complicated RNA-folding experiments in the future.

Although more work clearly needs to be done, our results suggest that both the double-strand stem and the single-strand loop significantly contribute for the 40A hairpin construct to the pressure-dependent response for the overall folding thermodynamics. Hairpin structures are ubiquitous in nucleic acids,[15,59] the response for which may help us understand pressure effects on more complex nucleic acid folding in extreme environments.[23] From our volumetric analysis, the positive ΔV°_{loop} is consistent with the disruption of base stacking within the poly(dA) linker, indicating that adjacent base stacking reduces the free volume of single-stranded DNA. On the other hand, the positive ΔV°_{stem} suggests that the DNA duplex formation increases the free volume. The two main forces that govern the structure of double-stranded DNA are inter-base-pair hydrogen bonding and base stacking. The overall positive sign for ΔV°_{stem} implies that inter-base-pair hydrogen bonding and perhaps higher-order structure formation (e.g., major and minor grooves) reduce solvent accessibility to the DNA backbone and thus lead to larger free volume,[60−62] completely dominating the volume reduction by base stacking.

IV.II. Deconstruction of Stem (ΔH_{stem}) and Loop (ΔH_{loop}) Enthalpy Changes. The enthalpy (ΔH°) and entropy (ΔS°) changes obtained from the temperature-dependent study in Section III.II are summarized in Figure 5B,C, respectively. For comparison, Figure 5B,C includes predictions from the so-called nearest-neighbor (NN) models, which take into account free energy contributions due to hydrogen bonding between single base pairs but also include the additional base stacking and stabilization effects accrued due to neighboring base pairs. The model parameters have been significantly improved and extended beyond Watson−Crick pairs in the past 2 decades and are now thought to provide reasonably accurate predictions of all thermodynamic parameters (ΔG, ΔH, and ΔS) for DNA duplexing.[24,25]

In Figure 5B, the experimental ΔH° values for hairpin folding and the nearest-neighbor predictions for duplex stem formation from two separate DNA strands (ΔH_{duplex}) clearly exhibit the same trend, specifically an increasing exothermicity with increasing number of base pairs (Figure 5B). However, there would also appear to be an equally clear and nearly constant shift between the two data sets, with $\Delta H^{\circ} - \Delta H_{duplex} \approx$ 15 kcal/mol (Figures 5B and 6A). In a manner similar to linear deconstruction of free volume changes ($\Delta V^{\circ} = \Delta V^{\circ}_{stem} + \Delta V^{\circ}_{loop}$) into stem and loop contributions, it is interesting to speculate how such an enthalpy shift could again arise by virtue of loop formation. Specifically, the offset between the two experimental and theoretical enthalpy curves can be attributed to differences between (i) full bimolecular formation of a stem (i.e., from separate ssDNAs) and (ii) unimolecular diffusing of the two stems together to form a hairpin linked by the poly(dA) strand, the latter of which incurs additional enthalpic (and entropic; see Section IV.III) contributions due to loop formation in the single-stranded DNA linker. From this perspective, subtraction of ΔH°_{stem} from ΔH° (Figure 6A) would correspond to the additional loop formation enthalpy ΔH°_{loop}, which from the fits in Figure 5B can be estimated to be $\Delta H^{\circ}_{loop} \approx$ +15(2) kcal/mol. If we further assume this additional enthalpy penalty to be proportional to linker length, the looping enthalpy per nucleotide [ΔH°_{loop}/40 nt ≈

DOI: 10.1021/acs.jpcb.9b10131
J. Phys. Chem. B 2020, 124, 110−120

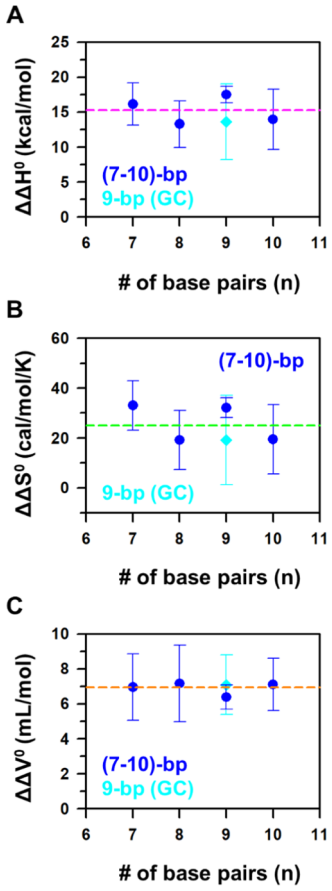

Figure 6. Subtraction of the stem length (n_{stem})-dependent contributions from DNA double-strand formation resulting in single-strand DNA looping (A) enthalpy (ΔH°_{loop}), (B) entropy (ΔS°_{loop}), and (C) free volume (ΔV°_{loop}) changes. The data is consistent with a simple linear offset for these loop contributions, indicated by pink, green, and orange dashed lines for enthalpy, entropy, and free volume, respectively.

+0.38(5) kcal/(mol nt)] would be relatively close to previously reported scaling relations (ΔH°_{loop} per nt ~ +0.5 kcal/(mol nt)) at comparable monovalent salt concentrations.[51] The source of such endothermicity could again be attributed to disrupted base stacking and distortion in the poly(dA) ssDNA loop.[51−55] Indeed, since a near-linear proportionality in incremental folding enthalpy has been observed in previous studies for constant stem lengths with linkers varying between 8 and 30 nucleotides,[51] our 20% lower per nucleotide value can be rationalized as due to partial relaxation of these looping distortions for a longer (40A) linker. Moreover, different buffer conditions may also contribute to our low ΔH°_{loop}; specifically, our experiments have been performed at lower monovalent cation concentrations ([M^+] = 100 vs 250 mM). This is quite relevant as base stacking is repressed at reduced [M^+],[52] thereby lowering the ΔH°_{loop} enthalpic penalty and is consistent with our observations. It is worth noting that such positive ΔH°_{loop} contributions again confirm that 40A loop formation is an endothermic process, enthalpically destabilizing the folded hairpin conformation.

IV.III. Deconstruction of Stem (ΔS_{stem}) and Loop (ΔS_{loop}) Entropy Changes. We can take this analysis one step further and attempt to deconstruct the entropic contributions for hairpin formation into both loop and stem components. In an analogous fashion to the trends in ΔH° (Figure 5B), the experimental dependence of ΔS° on sequence length (Figure 5C) follows a similar trend to that of nearest-neighbor model prediction,[24,25] with ΔS° systematically decreasing with increasing number of base pairs. The experimental results are again all shifted from model predictions by an approximately constant positive offset, which by a similar line of reasoning as in Section IV.II may be taken to represent the entropic contribution due to poly(dA) loop formation, i.e., ΔS°_{loop} = +25(7) cal/(mol K) (Figure 6B). Such entropic favoring of the looping process would again appear to be counterintuitive, since constraining the ends in a random walk or wormlike chain model would certainly lower the overall entropy.[49,50] However, in interpreting such an entropically favored loop formation, it is important to note that the poly(dA) linker contribution is more than simply structural. Specifically, the poly(dA) linker also plays a crucial role in raising the effective concentration of the one strand (S_2) with respect to its complement (S_1) and vice versa. Therefore, ΔS°_{loop} may be usefully deconstructed into two further contributions: (i) structural changes due to the biomolecule plus solvent system (ΔS°_{struct}) and (ii) unimolecular raising of the effective strand concentration (ΔS°_{conc}), with $\Delta S^\circ_{loop} = \Delta S^\circ_{conc} + \Delta S^\circ_{struct}$.

More quantitatively, the difference between the unimolecular folding equilibrium constant (K_{fold}) from covalently linked strands, i.e., what is experimentally measured, and a fully bimolecular duplex formation (K_{bimol}) from freely diffusing S_1, S_2 strands, i.e., what is predicted by the NN model, can be related as follows

$$K_{bimol} = \frac{[S_1S_2]}{[S_1][S_2]} = \frac{[S_1S_2]}{[S_1]} \times \frac{1}{[S_2]} = K_{fold} \times \frac{1}{[S_2]} \quad (6)$$

where [S_1], [S_2], and [S_1S_2] are concentrations of the two strands and the full hairpin, respectively.

For experimental folding of the 40A hairpin, an additional term of $RT\ln[S_2]_0$ between unimolecular and bimolecular folding free energies can be immediately recognized from the Gibbs relation $\Delta G^\circ = -RT\ln K_{fold}$. Such concentration effects are purely entropic, as the linker provides a physical limit to the phase space that S_2 can sample. The effective $[S_2]_0$ can be estimated from the random walk theory, where the 40-dA linker is simplified into a collection of N (~9) "Kuhn segments," with the angular orientation of a given Kuhn segment taken as completely random and independent of adjacent units.[63−65] The per volume probability density of the end-to-end distance for a random-walk polymer $P(r)$ is known to be well described by a Gaussian function,[66] with $P(r = 0)$ immediately recognized as the probability of S_1 and S_2 diffusing together. Therefore, the effective concentration is simply determined by matching the encounter probability $P(0)$ with a bulk concentration $[S_2]_0$. With previously determined persistence lengths and sizes of a single nucleotide base,[67−70] the effective concentration $[S_2]_0$ is calculated as 0.74(17) mM, corresponding to an additional entropy change of ΔS°_{conc} = +14.7(5) cal/(mol K) The positive sign of ΔS°_{conc} reflects the thermodynamic favoring of unimolecular over bimolecular folding due to entropic enhancement of the local strand concentration.

Consistent with our simple additive thermodynamic modeling, we can subtract this concentration entropy ΔS°_{conc} from the average linker contribution (ΔS°_{loop}) to infer an overall ΔS°_{struct} = +10(7) cal/(mol K) for structural change in

DOI: 10.1021/acs.jpcb.9b10131
J. Phys. Chem. B 2020, 124, 110−120

the poly(dA) linker plus solvent system. The positive value for ΔS°_{struct} implies an entropy increase when linear DNA turns into a loop via head-to-end connection. This entropy gain is at first counterintuitive, since the looping structure would be expected to restrict conformational phase space with respect to a linear configuration.[49,50] However, looping can also disrupt the low entropy state achieved by base stacking effects in the poly(dA) oligo. Consequently, distortion of base stacking due to loop formation could rationalize the observed entropy increase, arising from both translation and internal degrees of freedom such as bond rotation.[71] Indeed, such entropically favored unstacking between nucleotide bases has been previously reported for poly(dA) as well as between monomer dA bases.[71,72] Of course, the solvent entropy is an essential component of this estimate and must also be considered, since our measurements are only sensitive to entropy change of the combined solute + solvent system. However, solvation entropy would seem unlikely to explain the $\Delta S^\circ_{struct} > 0$, as compaction of the ring structure increases the overall charge density, subsequently stronger hydration forces, a more ordered water solvent environment, and thus $\Delta S^\circ_{solvent} < 0$.[73,74] In short, the entropy gain from base stacking dissociation would appear to dominate the overall favorable looping entropy, resulting in positive ΔS°_{struct}. It is interesting to note that positive entropy changes are also observed in a detailed molecular simulation study by Mishra et al.,[75] where the presence of an ssDNA linker entropically stabilizes the folded hairpin due to more prominent base stacking upon unfolding of the hairpin.[75]

In summary, the overall effect of the poly(dA) linker appears to be entropically favorable to hairpin folding ($\Delta S^\circ_{loop} > 0$). Part of this contribution arises from $\Delta S^\circ_{conc} > 0$ due simply to the increase in effective strand concentration for linked polymers, which results in a larger effective K_{fold} under unimolecular vs bimolecular DNA duplexing conditions. The remainder of the entropy contribution can be attributed to conformational changes in the linker, whereby the disruption of base stacking in the poly(dA) linker relaxes the configurational confinement in translational and internal degrees of freedom during looping, resulting in $\Delta S^\circ_{struct} > 0$. In the end, subtraction of $\Delta V^\circ_{stem} = \Delta V^\circ_{bp}$ [=+1.98(16) cm^3/(mol bp)] × n from the overall change in free volume ΔV° is also plotted in Figure 6C to highlight the loop contribution ΔV°_{loop}. In the context of this simple additive model, the thermodynamic properties (change in free volume, enthalpy, and entropy) of the isolated 9 bp stem and 40-dA loop are schematically summarized in Figure 7.

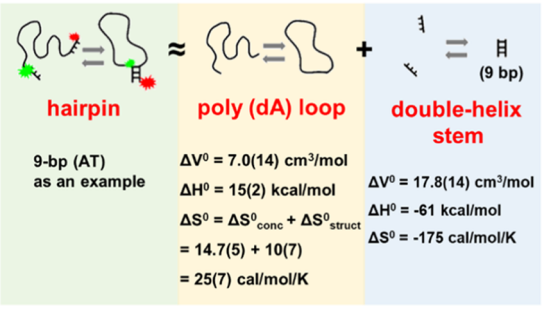

Figure 7. Summary of our simple additive model for deconstruction of the stem-length-dependent [9 bp (AT)] folding thermodynamics of a 40A DNA hairpin.

V. SUMMARY AND CONCLUSIONS

The thermodynamic properties (ΔH°, ΔS°, and ΔV°) of DNA hairpin folding have been studied via smFRET spectroscopy as a function of temperature, external pressure (1−3000 bar), and base-pair stem length. In the temperature-dependent studies, folding of these 40A DNA hairpin constructs is found to be exothermic ($\Delta H^\circ < 0$) with an entropic penalty ($\Delta S^\circ < 0$), with pressure-induced unfolding experiments indicating that the DNA hairpin takes up more volume in the folded vs unfolded state ($\Delta V^\circ > 0$). With such a high dynamic range in external pressure control (P_{ext} = 1−3000 bar), changes in free volume with single base-pair resolution have been achieved, allowing ΔV° for the DNA hairpins to be linearly deconstructed into stem [ΔV°_{bp} = +1.98(16) cm^3/(mol bp)] and loop [ΔV°_{loop} = +7.0(14) cm^3/mol] contributions by analyzing the dependence on length and complementary sequence. Based on predictions (ΔH°_{stem} and ΔS°_{stem}) from a nearest-neighbor model, both ΔH° and ΔS° for the full DNA hairpin can thereby be deconstructed into stem and loop contributions. It is found that single-strand loop formation is endothermic [ΔH°_{loop} = +15(2) kcal/mol] and yet compensated by positive entropic gain [ΔS°_{loop} = +25(7) cal/(mol K)], where the looping endothermicity can be attributed to the disruption of base stacking in the poly(dA) linker. In the context of a simple additive thermodynamic model, this positive ΔS°_{loop} can be further deconstructed into contributions due to unimolecular enhancement in the effective strand concentration [ΔS°_{conc} = +14.7(5) cal/(mol K)], with the remainder attributed to structural changes in the loop [ΔS°_{struct} = +10(7) cal/(mol K)] arising from the disruption of base stacking relaxing external (i.e., translational) and internal (i.e., hindered rotational) constraints.

AUTHOR INFORMATION

Corresponding Author

*E-mail: djn@jila.colorado.edu.

ORCID

David J. Nesbitt: 0000-0001-5365-1120

Notes

The authors declare no competing financial interest.

ACKNOWLEDGMENTS

The authors would like to thank Curtis Beimborn and Kenneth Wilson for help with the high-pressure experiment setup and many insightful discussions. Initial funding for this work has been provided by the National Science Foundation (CHE-1665271, PHY 1734006) and ongoing support from the Air Force Office of Scientific Research (FA9550-15-1-0090). We would also like to acknowledge early contributions by the W. M. Keck Foundation Initiative in RNA Sciences at the University of Colorado, Boulder. We would also like to acknowledge David Nicholson for his excellent help in editing the manuscript.

REFERENCES

(1) Heremans, K.; Smeller, L. Protein Structure and Dynamics at High Pressure. *Biochim. Biophys. Acta, Protein Struct. Mol. Enzymol.* **1998**, *1386*, 353−370.

(2) Smeller, L. Pressure−Temperature Phase Diagrams of Biomolecules. *Biochim. Biophys. Acta, Protein Struct. Mol. Enzymol.* **2002**, *1595*, 11−29.

DOI: 10.1021/acs.jpcb.9b10131
J. Phys. Chem. B 2020, 124, 110−120

(3) Mozhaev, V. V.; Heremans, K.; Frank, J.; Masson, P.; Balny, C. High Pressure Effects on Protein Structure and Function. *Proteins* **1996**, *24*, 81−91.
(4) Meersman, F.; Daniel, I.; Bartlett, D. H.; Winter, R.; Hazael, R.; McMillan, P. F. High-Pressure Biochemistry and Biophysics. *Rev. Mineral. Geochem.* **2013**, *75*, 607−648.
(5) Somero, G. N. Adaptations to High Hydrostatic Pressure. *Annu. Rev. Physiol.* **1992**, *54*, 557−577.
(6) Zhang, J.; Peng, X.; Jonas, A.; Jonas, J. NMR Study of the Cold, Heat, and Pressure Unfolding of Ribonuclease A. *Biochemistry* **1995**, *34*, 8631−8641.
(7) Jonas, J.; Ballard, L.; Nash, D. High-Resolution, High-Pressure NMR Studies of Proteins. *Biophys. J.* **1998**, *75*, 445−452.
(8) Schroer, M. A.; Paulus, M.; Jeworrek, C.; Krywka, C.; Schmacke, S.; Zhai, Y.; Wieland, D. C. F.; Sahle, C. J.; Chimenti, M.; Royer, C. A.; Garcia-Moreno, B.; Tolan, M.; Winter, R. High-Pressure SAXS Study of Folded and Unfolded Ensembles of Proteins. *Biophys. J.* **2010**, *99*, 3430−3437.
(9) Fujisawa, T.; Kato, M.; Inoko, Y. Structural Characterization of Lactate Dehydrogenase Dissociation under High Pressure Studied by Synchrotron High-Pressure Small-Angle X-ray Scattering. *Biochemistry* **1999**, *38*, 6411−6418.
(10) Krywka, C.; Sternemann, C.; Paulus, M.; Tolan, M.; Royer, C.; Winter, R. Effect of Osmolytes on Pressure-Induced Unfolding of Proteins: A High-Pressure SAXS Study. *ChemPhysChem* **2008**, *9*, 2809−2815.
(11) Patra, S.; Anders, C.; Erwin, N.; Winter, R. Osmolyte Effects on the Conformational Dynamics of a DNA Hairpin at Ambient and Extreme Environmental Conditions. *Angew. Chem., Int. Ed.* **2017**, *56*, 5045−5049.
(12) Smeller, L.; Fidy, J.; Heremans, K. Protein Folding, Unfolding and Aggregation. Pressure Induced Intermediate States on the Refolding Pathway of Horseradish Peroxidase. *J. Phys.: Condens. Matter* **2004**, *16*, S1053−S1058.
(13) Silva, J. L.; Oliveira, A. C.; Gomes, A. M. O.; Lima, L. M. T. R.; Mohana-Borges, R.; Pacheco, A. B. F.; Foguel, D. Pressure Induces Folding Intermediates that are Crucial for Protein−DNA Recognition and Virus Assembly. *Biochim. Biophys. Acta, Protein Struct. Mol. Enzymol.* **2002**, *1595*, 250−265.
(14) Patra, S.; Anders, C.; Schummel, P. H.; Winter, R. Antagonistic Effects of Natural Osmolyte Mixtures and Hydrostatic Pressure on the Conformational Dynamics of a DNA Hairpin Probed at the Single-Molecule Level. *Phys. Chem. Chem. Phys.* **2018**, *20*, 13159−13170.
(15) Bikard, D.; Loot, C.; Baharoglu, Z.; Mazel, D. Folded DNA in Action: Hairpin Formation and Biological Functions in Prokaryotes. *Microbiol. Mol. Biol. Rev.* **2010**, *74*, 570−588.
(16) Nicholson, D. A.; Sengupta, A.; Sung, H.-L.; Nesbitt, D. J. Amino Acid Stabilization of Nucleic Acid Secondary Structure: Kinetic Insights from Single-Molecule Studies. *J. Phys. Chem. B* **2018**, *122*, 9869−9876.
(17) Nakano, S.-i.; Yamaguchi, D.; Tateishi-Karimata, H.; Miyoshi, D.; Sugimoto, N. Hydration Changes upon DNA Folding Studied by Osmotic Stress Experiments. *Biophys. J.* **2012**, *102*, 2808−2817.
(18) Patra, S.; Schuabb, V.; Kiesel, I.; Knop, J.-M.; Oliva, R.; Winter, R. Exploring the Effects of Cosolutes and Crowding on the Volumetric and Kinetic Profile of the Conformational Dynamics of a Poly dA Loop DNA Hairpin: a Single-Molecule FRET Study. *Nucleic Acids Res.* **2018**, *47*, 981−996.
(19) Baltierra-Jasso, L. E.; Morten, M. J.; Laflör, L.; Quinn, S. D.; Magennis, S. W. Crowding-Induced Hybridization of Single DNA Hairpins. *J. Am. Chem. Soc.* **2015**, *137*, 16020−16023.
(20) Stiehl, O.; Weidner-Hertrampf, K.; Weiss, M. Kinetics of Conformational Fluctuations in DNA Hairpin-Loops in Crowded Fluids. *New J. Phys.* **2013**, *15*, No. 113010.
(21) Knowles, D. B.; LaCroix, A. S.; Deines, N. F.; Shkel, I.; Record, M. T. Separation of Preferential Interaction and Excluded Volume Effects on DNA Duplex and Hairpin Stability. *Proc. Natl. Acad. Sci. U.S.A.* **2011**, *108*, 12699−12704.
(22) Varani, G. Exceptionally Stable Nucleic Acid Hairpins. *Annu. Rev. Biophys. Biomol. Struct.* **1995**, *24*, 379−404.
(23) SantaLucia, J.; Hicks, D. The Thermodynamics of DNA Structural Motifs. *Annu. Rev. Biophys. Biomol. Struct.* **2004**, *33*, 415−440.
(24) SantaLucia, J.; Allawi, H. T.; Seneviratne, P. A. Improved Nearest-Neighbor Parameters for Predicting DNA Duplex Stability. *Biochemistry* **1996**, *35*, 3555−3562.
(25) SantaLucia, J. A Unified View of Polymer, Dumbbell, and Oligonucleotide DNA Nearest-Neighbor Thermodynamics. *Proc. Natl. Acad. Sci. U.S.A.* **1998**, *95*, 1460−1465.
(26) Rauzan, B.; McMichael, E.; Cave, R.; Sevcik, L. R.; Ostrosky, K.; Whitman, E.; Stegemann, R.; Sinclair, A. L.; Serra, M. J.; Deckert, A. A. Kinetics and Thermodynamics of DNA, RNA, and Hybrid Duplex Formation. *Biochemistry* **2013**, *52*, 765−772.
(27) Tekmen, M.; Müller, J. D. High-Pressure Cell for Fluorescence Fluctuation Spectroscopy. *Rev. Sci. Instrum.* **2004**, *75*, 5143−5148.
(28) Beimborn, J. C.; Hall, L. M. G.; Tongying, P.; Dukovic, G.; Weber, J. M. Pressure Response of Photoluminescence in Cesium Lead Iodide Perovskite Nanocrystals. *J. Phys. Chem. C* **2018**, *122*, 11024−11030.
(29) Fiore, J. L.; Kraemer, B.; Koberling, F.; Edmann, R.; Nesbitt, D. J. Enthalpy-Driven RNA Folding: Single-Molecule Thermodynamics of Tetraloop−Receptor Tertiary Interaction. *Biochemistry* **2009**, *48*, 2550−2558.
(30) Sengupta, A.; Sung, H.-L.; Nesbitt, D. J. Amino Acid Specific Effects on RNA Tertiary Interactions: Single-Molecule Kinetic and Thermodynamic Studies. *J. Phys. Chem. B* **2016**, *120*, 10615−10627.
(31) Vieweger, M.; Holmstrom, Erik D.; Nesbitt, D. J. Single-Molecule FRET Reveals Three Conformations for the TLS Domain of Brome Mosaic Virus Genome. *Biophys. J.* **2015**, *109*, 2625−2636.
(32) Sung, H.-L.; Nesbitt, D. J. Novel Heat-Promoted Folding Dynamics of the *yybP-ykoY* Manganese Riboswitch: Kinetic and Thermodynamic Studies at the Single-Molecule Level. *J. Phys. Chem. B* **2019**, *123*, 5412−5422.
(33) Fiore, J. L.; Hodak, J. H.; Piestert, O.; Downey, C. D.; Nesbitt, D. J. Monovalent and Divalent Promoted GAAA Tetraloop-Receptor Tertiary Interactions from Freely Diffusing Single-Molecule Studies. *Biophys. J.* **2008**, *95*, 3892−3905.
(34) Fiegland, L. R.; Garst, A. D.; Batey, R. T.; Nesbitt, D. J. Single-Molecule Studies of the Lysine Riboswitch Reveal Effector-Dependent Conformational Dynamics of the Aptamer Domain. *Biochemistry* **2012**, *51*, 9223−9233.
(35) Macgregor, R. B., Jr. Effect of Hydrostatic Pressure on Nucleic Acids. *Biopolymers* **1998**, *48*, 253−263.
(36) Roche, J.; Royer, C. A. Lessons from Pressure Denaturation of Proteins. *J. R. Soc., Interface* **2018**, *15*, No. 20180244.
(37) Roche, J.; Caro, J. A.; Norberto, D. R.; Barthe, P.; Roumestand, C.; Schlessman, J. L.; Garcia, A. E.; García-Moreno E, B.; Royer, C. A. Cavities Determine the Pressure Unfolding of Proteins. *Proc. Natl. Acad. Sci. U.S.A.* **2012**, *109*, 6945−6950.
(38) Nucci, N. V.; Fuglestad, B.; Athanasoula, E. A.; Wand, A. J. Role of Cavities and Hydration in the Pressure Unfolding of T_4 Lysozyme. *Proc. Natl. Acad. Sci. U.S.A.* **2014**, *111*, 13846−13851.
(39) Rashin, A. A.; Iofin, M.; Honig, B. Internal Cavities and Buried Waters in Globular Proteins. *Biochemistry* **1986**, *25*, 3619−3625.
(40) Najaf-Zadeh, R.; Wu, J. Q.; Macgregor, R. B. Effect of Cations on the Volume of the Helix-Coil Transition of Poly[d(A-T)]. *Biochim. Biophys. Acta, Gene Struct. Expression* **1995**, *1262*, 52−58.
(41) Rayan, G.; Macgregor, R. B. Pressure-Induced Helix−Coil Transition of DNA Copolymers is Linked to Water Activity. *Biophys. Chem.* **2009**, *144*, 62−66.
(42) Rayan, G.; Macgregor, R. B. A Look at the Effect of Sequence Complexity on Pressure Destabilisation of DNA Polymers. *Biophys. Chem.* **2015**, *199*, 34−38.
(43) Lane, A. N.; Jenkins, T. C. Thermodynamics of Nucleic Acids and Their Interactions with Ligands. *Annu. Rev. Biophys.* **2001**, *33*, 255−306.

DOI: 10.1021/acs.jpcb.9b10131
J. Phys. Chem. B 2020, 124, 110−120

(44) McConnell, T. S.; Cech, T. R. A Positive Entropy Change for Guanosine Binding and for the Chemical Step in the Tetrahymena Ribozyme Reaction. *Biochemistry* **1995**, *34*, 4056−4067.
(45) Mikulecky, P. J.; Feig, A. L. Cold Denaturation of the Hammerhead Ribozyme. *J. Am. Chem. Soc.* **2002**, *124*, 890−891.
(46) Lumry, R.; Rajender, S. Enthalpy−Entropy Compensation Phenomena in Water Solutions of Proteins and Small Molecules: A Ubiquitous Properly of Water. *Biopolymers* **1970**, *9*, 1125−1227.
(47) Schmid, R.; Miah, A. M.; Sapunov, V. N. A New Table of the Thermodynamic Quantities of Ionic Hydration: Values and Some applications (Enthalpy−Entropy Compensation and Born Radii). *Phys. Chem. Chem. Phys.* **2000**, *2*, 97−102.
(48) Wu, J. Q.; Macgregor, R. B., Jr. Pressure Dependence of the Helix−Coil Transition Temperature of Poly[d(G-C)]. *Biopolymers* **1995**, *35*, 369−376.
(49) Allemand, J.-F.; Cocco, S.; Douarche, N.; Lia, G. Loops in DNA: An Overview of Experimental and Theoretical Approaches. *Eur. Phys. J. E* **2006**, *19*, 293−302.
(50) Hanke, A.; Metzler, R. Entropy Loss in Long-Distance DNA Looping. *Biophys. J.* **2003**, *85*, 167−173.
(51) Goddard, N. L.; Bonnet, G.; Krichevsky, O.; Libchaber, A. Sequence Dependent Rigidity of Single Stranded DNA. *Phys. Rev. Lett.* **2000**, *85*, 2400−2403.
(52) Plumridge, A.; Meisburger, S. P.; Andresen, K.; Pollack, L. The Impact of Base Stacking on the Conformations and Electrostatics of Single-Stranded DNA. *Nucleic Acids Res.* **2017**, *45*, 3932−3943.
(53) Ke, C.; Humeniuk, M.; S-Gracz, H.; Marszalek, P. E. Direct Measurements of Base Stacking Interactions in DNA by Single-Molecule Atomic-Force Spectroscopy. *Phys. Rev. Lett.* **2007**, *99*, No. 018302.
(54) Mosayebi, M.; Romano, F.; Ouldridge, T. E.; Louis, A. A.; Doye, J. P. K. The Role of Loop Stacking in the Dynamics of DNA Hairpin Formation. *J. Phys. Chem. B* **2014**, *118*, 14326−14335.
(55) Buhot, A.; Halperin, A. Effects of Stacking on the Configurations and Elasticity of Single-Stranded Nucleic Acids. *Phys. Rev. E* **2004**, *70*, No. 020902.
(56) Yancey, P. H.; Blake, W. R.; Conley, J. Unusual Organic Osmolytes in Deep-Sea Animals: Adaptations to Hydrostatic Pressure and Other Perturbants. *Comp. Biochem. Physiol., Part A: Mol. Integr. Physiol.* **2002**, *133*, 667−676.
(57) Yancey, P. H.; Gerringer, M. E.; Drazen, J. C.; Rowden, A. A.; Jamieson, A. Marine Fish May be Biochemically Constrained from Inhabiting the Deepest Ocean Depths. *Proc. Natl. Acad. Sci. U.S.A.* **2014**, *111*, 4461−4465.
(58) Holmstrom, E. D.; Dupuis, N. F.; Nesbitt, D. J. Kinetic and Thermodynamic Origins of Osmolyte-Influenced Nucleic Acid Folding. *J. Phys. Chem. B* **2015**, *119*, 3687−3696.
(59) Svoboda, P.; Cara, A. D. Hairpin RNA: A Secondary Structure of Primary Importance. *Cell. Mol. Life Sci.* **2006**, *63*, 901−908.
(60) Alden, C. J.; Kim, S.-H. Solvent-accessible surfaces of nucleic acids. *J. Mol. Biol.* **1979**, *132*, 411−434.
(61) Pal, S.; Maiti, P. K.; Bagchi, B.; Hynes, J. T. Multiple Time Scales in Solvation Dynamics of DNA in Aqueous Solution: The Role of Water, Counterions, and Cross-Correlations. *J. Phys. Chem. B* **2006**, *110*, 26396−26402.
(62) Auffinger, P.; Hashem, Y. Nucleic Acid Solvation: From Outside to Insight. *Curr. Opin. Struct. Biol.* **2007**, *17*, 325−333.
(63) Kuhn, W. Über die Gestalt fadenförmiger Moleküle in Lösungen. *Kolloid-Z.* **1934**, *68*, 2−15.
(64) Kuhn, W.; Kuhn, H. Die Frage nach der Aufrollung von Fadenmolekeln in strömenden Lösungen. *Helv. Chim. Acta* **1943**, *26*, 1394−1465.
(65) Vologodskii, A. *Biophysics of DNA*; Cambridge University Press: Cambridge, 2015.
(66) Doi, M.; See, H. *Introduction to Polymer Physics*; Oxford Univesity Press: New York, 1996.
(67) Chi, Q.; Wang, G.; Jiang, J. The Persistence Length and Length per Base of Single-Stranded DNA Obtained from Fluorescence Correlation Spectroscopy Measurements Using Mean Field Theory. *Phys. A* **2013**, *392*, 1072−1079.
(68) Kuznetsov, S. V.; Shen, Y.; Benight, A. S.; Ansari, A. A Semiflexible Polymer Model Applied to Loop Formation in DNA Hairpins. *Biophys. J.* **2001**, *81*, 2864−2875.
(69) Murphy, M. C.; Rasnik, I.; Cheng, W.; Lohman, T. M.; Ha, T. Probing Single-Stranded DNA Conformational Flexibility Using Fluorescence Spectroscopy. *Biophys. J.* **2004**, *86*, 2530−2537.
(70) Seol, Y.; Skinner, G. M.; Visscher, K.; Buhot, A.; Halperin, A. Stretching of Homopolymeric RNA Reveals Single-Stranded Helices and Base-Stacking. *Phys. Rev. Lett.* **2007**, *98*, No. 158103.
(71) Searle, M. S.; Williams, D. H. On the Stability of Nucleic Acid Structures in Solution: Enthalpy - Entropy Compensations, Internal Rotations and Reversibility. *Nucleic Acids Res.* **1993**, *21*, 2051−2056.
(72) Brahms, J.; Michelson, A. M.; Van Holde, K. E. Adenylate Oligomers in Single- and Double-Strand Conformation. *J. Mol. Biol.* **1966**, *15*, 467−488.
(73) Huber, R. G.; Fuchs, J. E.; von Grafenstein, S.; Laner, M.; Wallnoefer, H. G.; Abdelkader, N.; Kroemer, R. T.; Liedl, K. R. Entropy from State Probabilities: Hydration Entropy of Cations. *J. Phys. Chem. B* **2013**, *117*, 6466−6472.
(74) Marcus, Y. Thermodynamics of Ion Hydration and its Interpretation in Terms of a Common Model. *Pure Appl. Chem.* **1987**, *59*, 1093.
(75) Mishra, G.; Giri, D.; Li, M. S.; Kumar, S. Role of Loop Entropy in the Force Induced Melting of DNA Hairpin. *J. Chem. Phys.* **2011**, *135*, No. 035102.

DOI: 10.1021/acs.jpcb.9b10131
J. Phys. Chem. B 2020, 124, 110−120